YCl_3-substituted $CsPbI_3$ Perovskite Nanorods for Efficient Red Light-emitting Diodes

Muhammad Imran Saleem , Amarja Katware , Al Amin , Seo-Hee Jung , Jeong-Hwan Lee *

Posted Date: 23 March 2023

doi: 10.20944/preprints202303.0404.v1

Keywords: Anisotropic Growth; YCl₃-substituted Perovskite; 1D Nanorods; Transition Dipole Moments; Outcoupling Efficiency

Article

YCl_3-substituted $CsPbI_3$ Perovskite Nanorods for Efficient Red Light-emitting Diodes

Muhammad Imran Saleem [1], Amarja Katware [2], Al Amin [2], Seo-Hee Jung [2] and Jeong-Hwan Lee [1,2,*]

[1] 3D Convergence Center, Inha University, Incheon, 22212 Republic of Korea
[2] Department of Materials Science and Engineering, Inha University, Incheon, 22212 Republic of Korea
* Correspondence: jeong-hwan.lee@inha.ac.kr

Abstract: Cesium lead iodide ($CsPbI_3$) perovskite nanocrystals (NCs) are a promising material for red light-emitting diodes (LEDs) due to their excellent color-purity and high luminous efficiency. However, small-sized $CsPbI_3$ colloidal NCs, such as nanocubes, used in LEDs suffer from confinement effects, negatively impacting their photoluminescence quantum yield (PLQY) and overall efficiency. Here, we introduced YCl_3 into the $CsPbI_3$ perovskite, which formed anisotropic, one-dimensional (1D) nanorods. This was achieved by taking advantage of the difference in bond energies between Cl^- and I^- ions, which caused YCl_3 to promote the anisotropic growth of $CsPbI_3$ NCs. The YCl_3-based nanorods improved the PLQY and storage stability by passivating the defects reducing the nonradiative recombination rates. When the YCl_3-substituted $CsPbI_3$ nanorods are applied to the emissive layer in LEDs, we achieve an external quantum efficiency of ~3.16% which is 1.86-fold higher than the pristine $CsPbI_3$ NCs (1.69%) based LED. Notably, the ratio of horizontal transition dipole moments (TDMs) in the anisotropic YCl_3:$CsPbI_3$ nanorods was determined to be 75%, which is higher than the isotropically oriented TDMs in $CsPbI_3$ nanocrystals (67%). This increased TDM ratio led to higher light outcoupling efficiency in nanorods-based LEDs. Overall, the results suggest that YCl_3-substituted $CsPbI_3$ nanorods could be promising for achieving high-performance perovskite LEDs.

Keywords: Anisotropic Growth; YCl_3-substituted Perovskite; 1D Nanorods; Transition Dipole Moments; Outcoupling Efficiency

1. Introduction

Metal halide perovskites (MHPs) have gained significant attention due to their outstanding figures of merit, including remarkable color purity, efficient radiative recombination, tailorable emission wavelengths, and low-cost solution-processibility. As a result, they are considered a promising candidate for next-generation display and lighting [1–4]. Among various MHPs, all-inorganic $CsPbI_3$ nanocrystals (NCs) are crucial for these purposes owing to their outstanding chemical and thermal durability [5]. Recent strategies, such as morphology and interfacial control, architecture engineering, and surface chemistry engineering, have been implemented to improve the practical applications of $CsPbI_3$ NCs, boosting the external quantum efficiency (EQE) of $CsPbI_3$ NCs-based light-emitting diodes (LEDs) [6]. Despite the rapid progress, the $CsPbI_3$ NCs LEDs endure substantial limitations due to the small-sized (0-dimension NCs), attributed to the confinement effect [7]. The defects-enriched surface of colloidal $CsPbI_3$ NCs, owing to their small size, has a deleterious effect not exclusively limited to photoluminescence quantum yield (PLQY), but also coupled with the low-luminous efficiency of LEDs [8]. Moreover, the large surface area of small-size $CsPbI_3$ NCs requires excessive native ligands to passivate, which forms an insulation layer to impede the effective carrier transport capability in assembled NCs film are numerous arduous challenges that are correlated with $CsPbI_3$ NCs based LEDs [2].

Anisotropic one-dimensional (1D) nanorods can overcome the limitations of conventional $CsPbI_3$ NCs-based LEDs. This is because 1D nanorods combine two-directional quantum confinement effects with a significantly reduced surface trap density, leading to excellent photophysical properties and high aspect ratios [9]. The 1D nanorods possess excellent photophysical

 doi:10.20944/preprints202303.0404.v1

properties and high aspect ratios from their unique surface morphology [10,11]. Additionally, the well-defined morphology of 1D nanorods has the ability to confine the active area of charge carriers and shorten the transmission of carriers [3], making them more conducive to the exploration of efficient LEDs compared with their counterpart nanocrystals [12].

While recent reports have described the synthesis of perovskite nanorods from the water-oil transformation of Cs_4PbBr_6 polyhedrons into nanorods or fragmentation of perovskite nanowires initiated by anion-exchange processes [13,14], these methods result in impure morphologies and defects-enriched surfaces. Therefore, it remains challenging to directly synthesize perovskite nanorods with efficient radiative recombination rates (high PLQY) and well-defined aspect ratios. Importantly, the anisotropic nature of these nanorods' emissive layer is valuable to further increase the outcoupling efficiency by overcoming the photons losses that become trapped through waveguiding and total internal, prized for their high ratios of horizontal transition dipole moments (TDMs), contrary to isotopically oriented nanocubes (nanocrystals) [15–17].

Here, an unconventional approach is introduced based on yttrium (III) chloride hexahydrate ($YCl_3.6H_2O$) YCl3-substituted $CsPbI_3$ nanorods. The YCl_3-substituted $CsPbI_3$ nanorods decrease the lattice parameter of $CsPbI_3$ NCs owing to partial substitution of Pb^{2+} and I^- with bigger radius by smaller Cl^- ions. The YCl_3 passivates surface traps and regulates the net recombination rates, significantly improving PLQY. Importantly, the environmental durability of the YCl_3-substituted $CsPbI_3$ NRs improved significantly, losing 28% PLQY after being stored for 45 days under ambient conditions. Notably, the YCl_3:$CsPbI_3$-nanorod-based LEDs demonstrated a peak EQE of 3.16%, 1.86-fold higher than the control $CsPbI_3$ NCs-based device (1.69%). Importantly, the ratio of horizontal transition dipole moments of the anisotropic YCl_3:$CsPbI_3$ nanorods is determined to be 75%, which is higher than that of the isotopically oriented TDMs in $CsPbI_3$ nanocrystals (67%), resulting in higher light outcoupling efficiency. Our finding suggests that anisotropic nanorods have a promising prospect in light-emitting devices.

2. Materials and Methods

2.1. Synthesis of unsubstituted and YCl_3-substituted $CsPbI_3$ NCs

The previously reported hot-injection method was employed to synthesize the unsubstituted and YCl_3-substituted $CsPbI_3$ NCs [18,19].

2.1.1. Cesium Oleate Preparation

Firstly, Cs_2CO_3 (2.49 mmol), OLA (2.5 mL), and 30 mL ODE were degassed and dried at 120 °C for 1 h. Subsequently, the temperature was raised to 150 °C until a clear solution was obtained under N_2 flow.

2.1.2. Synthesis of $CsPbI_3$ NCs

PbI_2 (0.174 g, 0.376 mmol) and ODE (10 mL) were loaded into a 50 mL three-neck flask, degassed, and dried under vacuum for 1 h at 120 °C. Then, OA (1 mL), and OLA (1 mL) preheated to 70 °C were injected under the protection of N_2. After the solution became clear, the temperature was raised to 170 °C, and 0.8~1 mL Cs-oleate (pre-heated to >100 °C) was swiftly injected, which was quenched by immersing the flask in an ice-water bath (5 sec later).

2.1.3. Synthesis of YCl_3:$CsPbI_3$ NRs

ODE (10 mL), OA (1 mL), and $YCl_3{\cdot}6H_2O$ (0.184 mmol) were loaded into a three-neck flask and adequately dissolved at 150 °C for 1 h under N_2 flow. Then, PbI_2 (0.174 g, 0.376 mmol) and OLA were added, and the temperature was raised to 170 °C (30 min later). Then, as-prepared Cs-oleate was quickly injected into the mixture, and 60~65 s later, the reaction was quenched by immersing the flask in an ice-water bath [12].

 doi:10.20944/preprints202303.0404.v1

2.1.4. Purification

The unsubstituted and YCl_3-substituted $CsPbI_3$ NCs were separated by centrifugation at 5000 rpm for 10 min to remove the ODE and unreacted ligands. The precipitate was dispersed in hexane/toluene, and then anti-solvent methyl acetate was mixed, followed by centrifugation at 10000 rpm for 10 min. The resultant mixture was dispersed in 10 mL hexane/toluene and stored in the refrigerator. After 24 h, the supernatant required colloidal ink for LEDs application.

2.2. LED Fabrication

150-nm-thick Indium tin oxide (ITO) patterned glass substrates were cleaned by sequential ultrasonication in acetone and isopropanol for 15 min each. Further, the UV-ozone treatment was carried out for 15 min to improve hydrophilicity before drying with N_2 flow. PEDOT:PSS (filtered with 0.45 μm PVDF filter) was then spin-coated for 1 min at 4000 rpm, which was then annealed at 140 °C for 30 min. All the substrates were transferred into the N_2 glove box. The hole-transporting Poly-TPD (4 mg/mL in CB) layer was spin-coating onto PEDOT:PSS films at 4000 rpm and baked at 120 °C for 15~20 min. The perovskite emissive layer was spin-coated at a speed of 2000 rpm for 45 s. Then, 1,3,5-tris(1-phenyl-1H-benzimidazol-2-yl)benzene (TPBi, 40 nm), LiF (1 nm), and Al (130 nm) were sequentially deposited by thermal evaporation in a vacuum deposition chamber. A glass lid encapsulated all the devices with a UV-curable resin in an N_2-filled glovebox. The optoelectronic properties of LEDs were analyzed using a semiconductor parameter analyzer (Keithley 237) connected with a spectrophotometer (Photo Research PR-670). UV-Vis-IR absorption spectrum of the unsubstituted and YCl_3-substituted $CsPbI_3$ NCs film was tested using a PerkinElmer LAMBDA-900 spectrophotometer. PLQY was measured by Quantaurus-QY Absolute PL quantum yield spectrometer (Hamamatsu, C11347-11). The structure of the unsubstituted and YCl_3-substituted $CsPbI_3$ NCs thin film was analyzed by an X-ray diffractometer (X'Pert-PRO MRD, Phillips). The shape of the unsubstituted and YCl_3-substituted $CsPbI_3$ NCs was confirmed using a field-emission transmission electron microscope (FE-TEM, JEM-2100F) and the cross-sectional TEM images of the LED were obtained from a Cs-corrected TEM (JEM-ARM 200F, JEOL) installed in the Center for University-wide Research Facilities (CURF) at Jeonbuk National University. Chemical analysis was conducted by X-ray Photoelectron Spectrometer (XPS).

3. Results and Discussion

The control (unsubstituted) and YCl_3-substituted $CsPbI_3$ NCs were synthesized following the two-step hot-injection method [20]. The YCl_3-doped $CsPbI_3$ NRs were realized by adding 0.184 mmol of $YCl_3{\cdot}6H_2O$ into perovskite medium followed by the injection of Cs-oleate precursor **(Scheme 1a**). Unlike the previous reports that aimed at metal chlorides that used either the same or adjacent chloride element in the pristine perovskite NCs [14,21]. This study examines how metal chloride can modulate the shape and optoelectronic properties of $CsPbI_3$ NCs. Besides changing the surface defect of perovskite NCs, the YCl_3-doping has an additional effect on inducing the anisotropic growth of the crystals. The intention doping of YCl_3 was carried out in the $CsPbI_3$ NCs reaction medium; the distinctive chloride (Cl^-) was not adjacent to the iodide (I^-) of the $CsPbI_3$ NCs. The presence of chloride on the surface of perovskite nanocrystals (NCs) and the varied bond energies between Cl^- ions and I^- ions are responsible for the anisotropic growth of perovskite NCs. **(Scheme 1b)**. The transmission electron microscopy (TEM) analyses provide evidence to support this conjecture, as shown in **Figure 1**. The TEM and high resolution (HR-TEM) morphology of the control and YCl_3-substituted $CsPbI_3$ NCs revealed by TEM (Figure 1). The control $CsPbI_3$ NCs contain monodisperse and regular cubic shape (Figure 1a). The HR-TEM images show a high crystallinity and lattice spacing of 6.2 Å of the $CsPbI_3$ NCs, corresponding to the (100) plane of cubic perovskite (Figure 1b-c) [22,23]. The average particle size of the control $CsPbI_3$ NCs is determined to be ~10.05 nm (Figure 1d). Remarkably, the 0.184 mmol YCl_3-substituted $CsPbI_3$ NCs show the one-dimensional nanorods (NRs) (Figure 1e-g). The HR-TEM image of YCl_3-substituted $CsPbI_3$ NRs displays a lattice spacing of 4.5 Å, corresponding

Preprints (www.preprints.org) | NOT PEER-REVIEWED | Posted: 23 March 2023 doi:10.20944/preprints202303.0404.v1

to the (110) plane of perovskite (Figure 1g) [12]. The aspect ratio of the YCl_3-substituted $CsPbI_3$ NCs is ~2.3, and the average sizes of length and diameter are 18.5 and 8.2 nm, respectively.

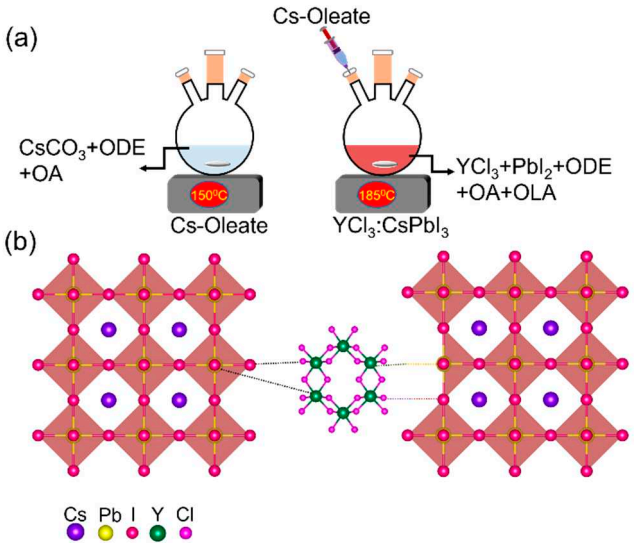

Scheme 1. (a) Schematic illustration of hot-injection method of YCl_3:$CsPbI_3$ NRs perovskite. **(b)** The intentional doping of YCl_3 in the perovskite reaction medium. The presence of the surface chloride initiates the unit cell's surface energy imbalance, leading to the anisotropic growth of $CsPbI_3$ NCs.

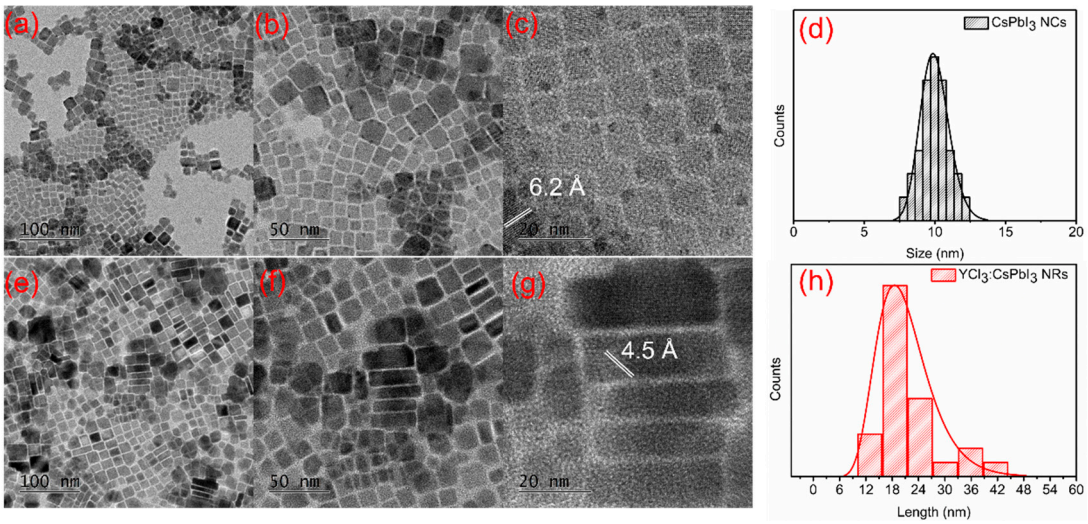

Figure 1. (a) TEM image, and **(b-c)** high-resolution TEM (HR-TEM) images of $CsPbI_3$ NCs. **(d)** The corresponding size distribution histograms. **(e)** TEM image, and **(f-g)** HR-TEM images of YCl_3-substituted $CsPbI_3$ NRs. **(h)** The corresponding size distribution histograms.

The X-ray diffraction (XRD) patterns were conducted to ascertain the crystal structure of $CsPbI_3$ NCs and YCl_3:$CsPbI_3$ NRs, as shown in **Figure 2.** Both the $CsPbI_3$ NCs and YCl_3:$CsPbI_3$ NRs adhere to the reference pattern of the bulk cubic $CsPbI_3$ perovskite (PDF#98-018-1288), and the diffraction peaks appear at 14.02°, 20.03°, 28.407°, 31.88°, 35.45°, 41.05°, and 51.63° are corresponding to cubic planes of (100), (110), (200), (210), (211), (220) and (300), respectively. The diffraction peaks of (100) and (200) planes shift toward higher angles attributed to the decrease of lattice parameters of YCl_3:$CsPbI_3$ NRs stemmed from the partial substitution Pb^{2+} and I^- with bigger radius by the smaller Y^{3+} and Cl^- ions, respectively [12,24]. The scanning electron microscopy (SEM) images of the unsubstituted and YCl_3-substituted $CsPbI_3$ NCs are illustrated in Figure 2b-c. Contrary to perovskite NCs, the SEM image of

Preprints (www.preprints.org) | NOT PEER-REVIEWED | Posted: 23 March 2023 doi:10.20944/preprints202303.0404.v1

(YCl_3-substituted $CsPbI_3$) nanorods are homogeneously distributed on a glass substrate, which indicates that the nanorod film layer has a good foundation for electroluminescent.

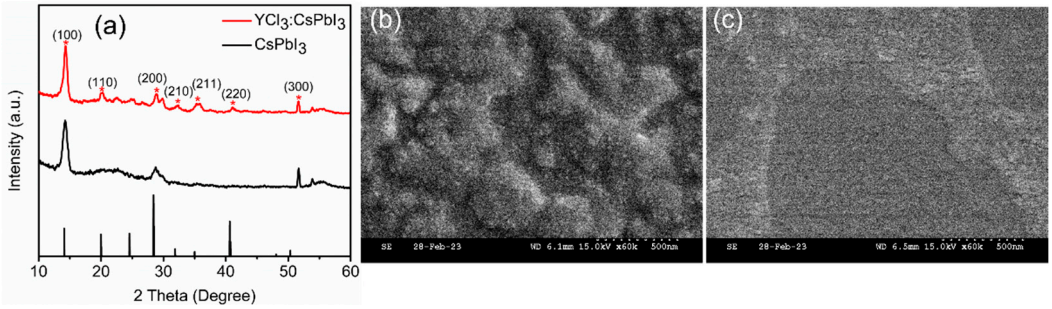

Figure 2. (a) TEM image, and **(b-c)** high-resolution TEM (HR-TEM) images of $CsPbI_3$ NCs. **(d)** The corresponding size distribution histograms. **(e)** TEM image, and **(f-g)** HR-TEM images of YCl_3-substituted $CsPbI_3$ NRs. **(h)** The corresponding size distribution histograms.

X-ray photoelectron spectra (XPS) analysis was performed to gain insight into the interaction of YCl_3 with $CsPbI_3$ nanocrystals (NCs), and the results are presented in Figure 3(a). The characteristic XPS signals for Cs 3d, Pb 4f, I 3d, Y 3d, and Cl 2p were observed in YCl_3-doped $CsPbI_3$ NCs and N 1s, O 1s, and C 1s signals coupled with native ligand bonding. The high-resolution XPS spectra of Cs 3d, Pb 4f, I 3d, Y 3d, and Cl 2p are displayed in Figure 3(b-f), respectively. The partial substitution of I^- ions by Cl^- ions is evidenced by an increase in the binding energies of Pb^{2+} $4f_{5/2}$ and Pb^{2+} $4f_{7/2}$ from 143.56 and 138.37 eV to 143.64 and 138.7 eV, respectively. The binding energy of I 3d and Cs 3d display little variation compared to YCl_3:$CsPbI_3$ nanocrystals (NCs). More importantly, the Y^{3+} and Cl^- binding energy signals can be observed in the YCl_3-substituted $CsPbI_3$ nanorods (NRs). These findings support the partial substitution of I^- ions by Cl^- ions [25].

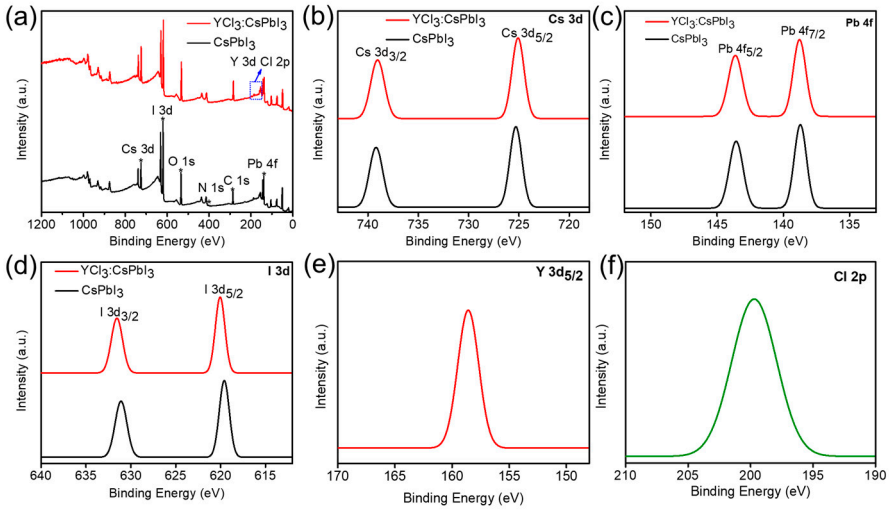

Figure 3. (a) X-ray photoelectron spectroscopy (XPS) of $CsPbI_3$ NCs and YCl_3:$CsPbI_3$ NRs. High resolution-XPS spectra of **(b)** Cs 3d, **(c)** Pb 4f, and **(d)** I 3d of pristine $CsPbI_3$ NCs and YCl_3:$CsPbI_3$ NRs. **(e-f)** Y 3d and Cl 2p spectra of YCl_3-substituted $CsPbI_3$ NRs thin film.

To gain a better understanding of the effects of partial substitution of Pb^{2+} cation and I^- with larger radius by the smaller Y^{3+} and Cl^- ions, the optical properties of both as-synthesized $CsPbI_3$ nanocrystals (NCs) and YCl_3:$CsPbI_3$ nanorods (NRs) were analyzed (**Figure 4**). The corresponding normalized PL and absorption spectra of YCl_3:$CsPbI_3$ NRs showed that peak position exhibited a blue-shift owing to partial substitution of Y^{3+} cation [26]. The enlarged bandgap caused the blue-shifts

Preprints (www.preprints.org) | NOT PEER-REVIEWED | Posted: 23 March 2023 doi:10.20944/preprints202303.0404.v1

of the absorption and PL spectra for YCl3:CsPbI3 NRs due to the partial substitution of Pb^{2+} cation and I^- with bigger radius by the smaller Y^{3+} and Cl^- ions [27]. The photoluminescence quantum yield (PLQY) increased from 51% to 70% for the 0.184 mmol YCl_3 passivated $CsPbI_3$ NCs, suggesting enhanced radiative recombination followed by yttrium chloride doping (**Figure 4c**). The ambient stability of the YCl_3:$CsPbI_3$ solution was noticeably improved (**Figure 4d**), the YCl_3-substituted $CsPbI_3$ NRs maintained (50% out of 70%) a PLQY, loss of 28% PLQY after being stored for 45 days under ambient condition, prized for the effectiveness of yttrium chloride passivation. However, over the same period of time, the PL quantum yield of pristine $CsPbI_3$ NCs nearly approached zero. The inset of **Figure 4d** shows the images recorded at different times for the unsubstituted and YCl_3-substituted $CsPbI_3$ NCs solution.

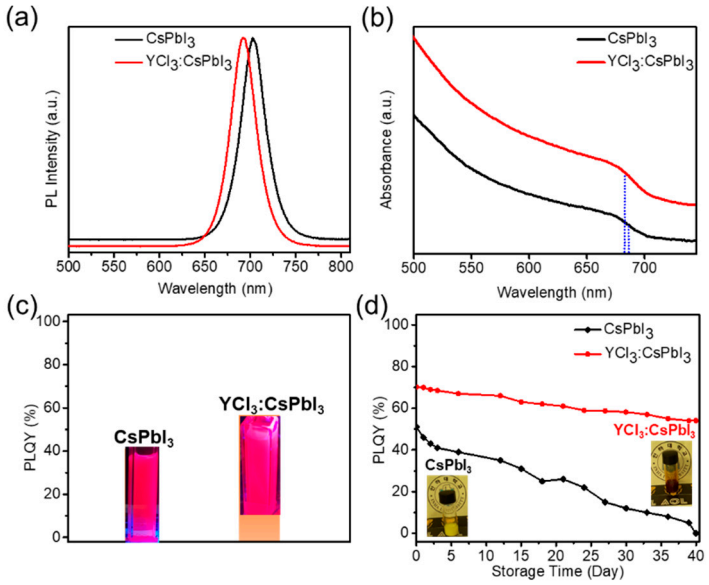

Figure 4. (a-c) Photoluminescence (PL), absorption spectra, and PL-quantum yield (PLQY) of the unsubstituted and YCl_3-substituted $CsPbI_3$ NCs. The inset **Figure 3(c)** is the image of the $CsPbI_3$ NCs and YCl_3:$CsPbI_3$ NRs solution under the UV lamp. **(d)** PLQY values as a function of stored days for unsubstituted and YCl_3-substituted $CsPbI_3$ NCs solution. The inset is real images of both samples after 45 days.

The control and YCl_3-substituted $CsPbI_3$ NCs were employed as emitters to evaluate the potential applications in perovskite LEDs. The LEDs were fabricated based on the configuration of indium tin oxide (ITO)/ poly(3,4-ethylenedioxythiophene) polystyrenesulfonate (PEDOT: PSS)/poly(4-butylphenyl-diphenyl-amine) (P-TPD)/ unsubstituted $CsPbI_3$ or YCl_3:$CsPbI_3$/ 1,3,5-tris(1-phenyl-1H-benzimidazol-2-yl)benzene (TPBi)/ lithium fluoride (LiF)/ aluminum (Al). The schematic illustration of PeLED, and the corresponding energy levels diagram of the functional layer are illustrated in **Figure 5a-b**. The functional layers' energy level values are taken from previous literature [12]. The thickness of ITO (150 nm), PEDOT: PSS, P-TPD (60 nm), YCl_3:$CsPbI_3$ (55 nm), TPBi (60 nm), and LiF/Al (130 nm) were analyzed by the cross-sectional TEM image, as shown in **Figure 5c**. The current density-voltage-luminance (*J-V-L*) curves of the unsubstituted and YCl_3-substituted $CsPbI_3$ NCs LEDs with a 4 mm^2 emitting area are displayed in **Figure 5d.** The turn-on voltage (where the luminance achieved 1 cd/m^2) is reduced from ~3.9 V to ~3.6 V for the YCl_3-substituted $CsPbI_3$ NCs LED, revealing that more balanced carrier injected owing to their matched-energy level with carrier transfer layer and enhanced conductivity induced by the YCl_3-substitution that facilitated the efficient charges injection [12,23]. The $CsPbI_3$ NCs and YCl_3:$CsPbI_3$ NRs-based LEDs showed a maximum luminance of 263.1 cd/m^2 and 421.8 cd/m^2, respectively. The electroluminescence (EL) spectra of the unsubstituted and YCl_3-substituted $CsPbI_3$ NCs LEDs were observed at 691 nm and 688 nm (**Figure 5e**). The YCl_3:$CsPbI_3$-based LEDs revealed high color purity with Commission

Preprints (www.preprints.org) | NOT PEER-REVIEWED | Posted: 23 March 2023 doi:10.20944/preprints202303.0404.v1

internationale de l'éclairage (CIE) coordinates of (0.71, 0.26), which corresponds to the BT. 2020 color gamut, as shown in **Figure 5f**. The EQE *vs.* luminance curves are displayed in **Figure 5g**. The peak EQE of YCl_3:$CsPbI_3$ is 3.16%, 1.86-fold higher than the pristine $CsPbI_3$ NCs (1.69%) based LED. This enhancement is attributed to enhanced PLQY and more balanced carrier transfer in the YCl_3:$CsPbI_3$ EML layer.

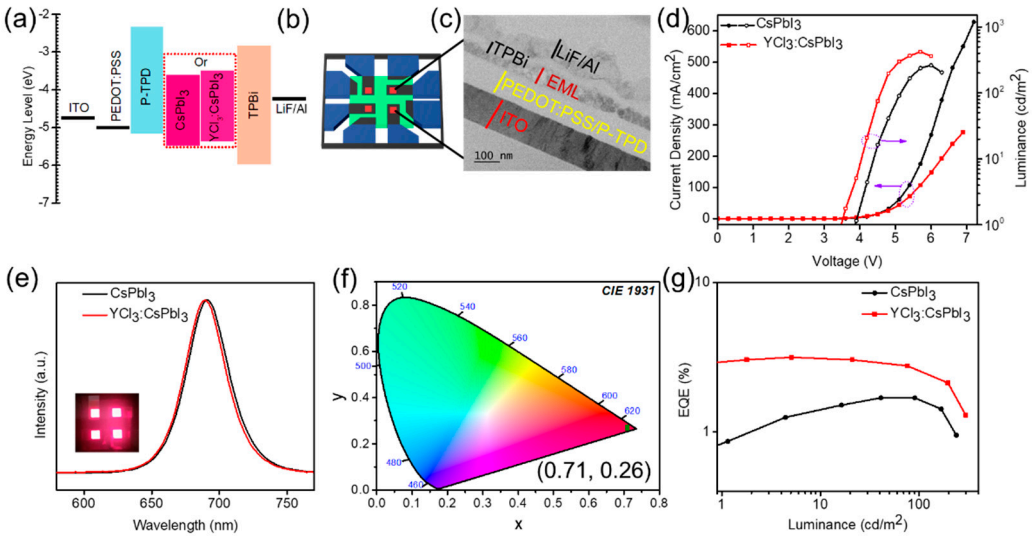

Figure 5. (a) Schematic flat-band energy diagram of perovskite LEDs. **(b-c)** Schematic device illustration and the corresponding cross-sectional TEM image of the perovskite LEDs. **(d)** Current density-voltage and luminance-voltage curves, **(e)** EL spectra of the unsubstituted and YCl_3-substituted $CsPbI_3$ LED device. The inset shows the image of a working YCl_3-substituted $CsPbI_3$ LED device. **(f)** The corresponding CIE coordinates for the EL spectrum (0.71, 0.26) of YCl_3-substituted $CsPbI_3$ LED. **(g)** EQE-Luminance curves of the unsubstituted and YCl_3-substituted $CsPbI_3$ LED device.

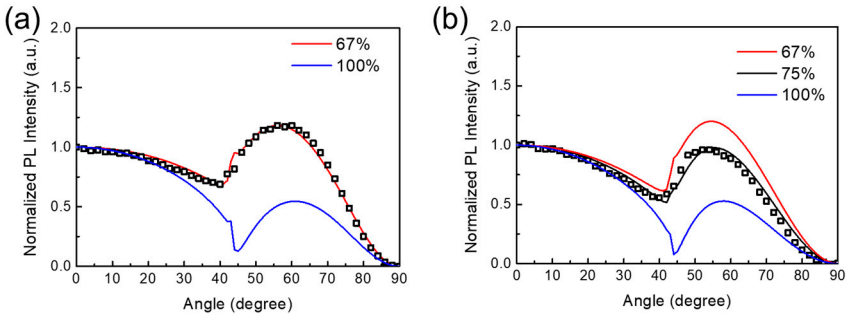

Figure 6. Angle-dependent PL measurements of the perovskite film on a quartz substrate/nanocrystal or nanorods. The experimental data (black squares) are fitted by the classical electromagnetic dipole model, giving a horizontal TDM ratio of **(a)** $CsPbI_3$ NCs 67%, and **(b)** YCl_3-substituted $CsPbI_3$ NRs 75%.

To further investigate the enhanced EQE in the YCl_3-substituted $CsPbI_3$ NRs, we conducted angle-dependent photoluminescence (ADPL) measurements to probe the orientation of transition dipole moments (TDMs) in the assembled thin film of $CsPbI_3$ nanocrystals/nanorods. The outcoupling efficiency in PeLEDs has the potential for improvement by controlling the orientation of TDMs [30]. The optical TDMs of nanoplatelets and nanorods are highly anisotropic, and outcoupling efficiency in planer PeLEDs is profoundly associated with the orientation of emissive TDMs [15,17]. The orientation of optical TDMs of the unsubstituted and YCl_3-substituted $CsPbI_3$ NCs was measured by the ratio of horizontal TDMs (Θ). The experimental data are fitted to the pattern simulated employing the classical dipole radiation model [31–34]. We confirmed that the Θ values of $CsPbI_3$

NCs and YCl_3:$CsPbI_3$ NRs film are determined to be 67% and 75% (**Figure 6a-b).** The Θ value in anisotropic nanorods is considerably higher than that of isotropic nanocrystals. Thus, the optical TDMs that are horizontally oriented in anisotropic nanorods are preferred for light outcoupling, resulting in the EQE of the LEDs.

4. Conclusions

In this study, we investigated the effects of incorporating metal chloride (YCl_3) into $CsPbI_3$ nanocrystals (NCs) to control the dimension. We found that incorporating YCl_3 led to a decrease in the lattice parameters of the $CsPbI_3$ NCs, which resulted from the partial substitution of larger Pb^{2+} and I^- ions with smaller Y^{3+} and Cl^- ions. The presence of Cl^- ions on the surface of the NCs, coupled with the difference in bond energies between Cl^- and I^- ions, led to the anisotropic growth of the $CsPbI_3$ NCs into one-dimensional (1D) nanorods. The YCl_3 also significantly improved the photoluminescence quantum yield and storage lifetime of the perovskite solution by properly passing nonradiative recombination rates and defects. Finally, we used the YCl_3-substituted $CsPbI_3$ nanorods as the emissive layer in red LEDs and observed a significant improvement in their performance. The LEDs exhibited an external quantum efficiency of 3.16% which is 1.86-fold higher than the pristine $CsPbI_3$ NCs (1.69%) based LED, attributed to the improvement of the ratio of horizontal TDMs in the anisotropic YCl_3:$CsPbI_3$ nanorods to 75% from 67% of that of NCs. Overall, the combined characteristics of YCl_3-substituted $CsPbI_3$ nanorods show great potential for developing stable and efficient red LEDs.

Author Contributions: M. I. Saleem: Conceptualization, investigation, data analysis, and writing—original draft preparation. A. Katware: Device fabrication. A. Amin: angle dependent PL analysis. S.-H. Jung: *J-V-L* characterization, J.-H. Lee: Conceptualization, writing—review and editing, supervision, funding acquisition. All authors have read and agreed to the published version of the manuscript.

Funding: This research was supported by Inha University Research Grant (No. 65380-1).

Data Availability Statement: Data will be made available upon request.

Acknowledgments: The authors would like to acknowledge Prof. Jae-Wook Kang from Department of Flexible and Printable Electronics, LANL-CBNU Engineering Institute-Korea, Jeonbuk National University) for Cs-corrected TEM measurement. In addition, we acknowledge the financial support provided by the Inha University Research Grant (No. 65380-1).

Conflicts of Interest: There is no conflict of interest.

References

1. Kim, Y.-H.; Kim, S.; Kakekhani, A.; Park, J.; Park, J.; Lee, Y.-H.; Xu, H.; Nagane, S.; Wexler, R.B.; Kim, D.-H.; et al. Comprehensive defect suppression in perovskite nanocrystals for high-efficiency light-emitting diodes. *Nat. Photonics* **2021**, *15*, 148-155, doi:10.1038/s41566-020-00732-4.
2. Yang, J.-N.; Chen, T.; Ge, J.; Wang, J.-J.; Yin, Y.-C.; Lan, Y.-F.; Ru, X.-C.; Ma, Z.-Y.; Zhang, Q.; Yao, H.-B. High Color Purity and Efficient Green Light-Emitting Diode Using Perovskite Nanocrystals with the Size Overly Exceeding Bohr Exciton Diameter. *J. Am. Chem. Soc.* **2021**, *143*, 19928-19937, doi:10.1021/jacs.1c09948.
3. Saleem, M.I.; Yang, S.; Batool, A.; Sulaman, M.; Veeramalai, C.P.; Jiang, Y.; Tang, Y.; Cui, Y.; Tang, L.; Zou, B. $CsPbI_3$ nanorods as the interfacial layer for high-performance, all-solution-processed self-powered photodetectors. *J. Mater. Sci. Technol.* **2021**, *75*, 196-204, doi:https://doi.org/10.1016/j.jmst.2020.07.049.
4. Saleem, M.I.; Yang, S.; Zhi, R.; Sulaman, M.; Chandrasekar, P.V.; Jiang, Y.; Tang, Y.; Batool, A.; Zou, B. Surface Engineering of All-Inorganic Perovskite Quantum Dots with Quasi Core–Shell Technique for High-Performance Photodetectors. *Adv. Mater. Interf.* **2020**, *7*, 2000360, doi:https://doi.org/10.1002/admi.202000360.
5. Shen, X.; Wang, Z.; Tang, C.; Zhang, X.; Lee, B.R.; Li, X.; Li, D.; Zhang, Y.; Hu, J.; Zhao, D.; et al. Near-Infrared LEDs Based on Quantum Cutting-Activated Electroluminescence of Ytterbium Ions. *Nano Lett.* **2023**, *23*, 82-90, doi:10.1021/acs.nanolett.2c03679.
6. Wang, Y.-K.; Yuan, F.; Dong, Y.; Li, J.-Y.; Johnston, A.; Chen, B.; Saidaminov, M.I.; Zhou, C.; Zheng, X.; Hou, Y.; et al. All-Inorganic Quantum-Dot LEDs Based on a Phase-Stabilized α-$CsPbI_3$ Perovskite. *Angew. Chem. Int. Ed.* **2021**, *60*, 16164-16170, doi:https://doi.org/10.1002/anie.202104812.

7. Polavarapu, L.; Nickel, B.; Feldmann, J.; Urban, A.S. Advances in Quantum-Confined Perovskite Nanocrystals for Optoelectronics. *Adv. Energy Mater.* **2017**, *7*, 1700267, doi:https://doi.org/10.1002/aenm.201700267.
8. Tang, C.; Shen, X.; Yu, S.; Zhong, Y.; Wang, Z.; Hu, J.; Lu, M.; Wu, Z.; Zhang, Y.; Yu, W.W.; et al. Post-treatment of $CsPbI_3$ nanocrystals by p-iodo-D-Phenylalanine for efficient perovskite LEDs. *Mater. Today Phys.* **2021**, *21*, 100555, doi:https://doi.org/10.1016/j.mtphys.2021.100555.
9. Bi, C.; Hu, J.; Yao, Z.; Lu, Y.; Binks, D.; Sui, M.; Tian, J. Self-Assembled Perovskite Nanowire Clusters for High Luminance Red Light-Emitting Diodes. *Adv. Funct. Mater.* **2020**, *30*, 2005990, doi:https://doi.org/10.1002/adfm.202005990.
10. Saleem, M.I.; Yang, S.; Zhi, R.; Li, H.; Sulaman, M.; Chandrasekar, P.V.; Zhang, Z.; Batool, A.; Zou, B. Self-powered, all-solution processed, trilayer heterojunction perovskite-based photodetectors. *Nanotechnology* **2020**, *31*, 254001, doi:10.1088/1361-6528/ab7de7.
11. Ji, R.; Zhang, Z.; Hofstetter, Y.J.; Buschbeck, R.; Hänisch, C.; Paulus, F.; Vaynzof, Y. Perovskite phase heterojunction solar cells. *Nat. Energy* **2022**, doi:10.1038/s41560-022-01154-y.
12. Pan, G.; Bai, X.; Shen, X.; Wang, L.; Mao, Y.; Chen, X.; Xu, W.; Shao, H.; Zhou, D.; Dong, B.; et al. Bright red YCl_3-promoted $CsPbI_3$ perovskite nanorods towards efficient light-emitting diode. *Nano Energy* **2021**, *81*, 105615, doi:https://doi.org/10.1016/j.nanoen.2020.105615.
13. Tong, Y.; Bladt, E.; Aygüler, M.F.; Manzi, A.; Milowska, K.Z.; Hintermayr, V.A.; Docampo, P.; Bals, S.; Urban, A.S.; Polavarapu, L.; et al. Highly Luminescent Cesium Lead Halide Perovskite Nanocrystals with Tunable Composition and Thickness by Ultrasonication. *Angew. Chem. Int. Ed.* **2016**, *55*, 13887-13892, doi:https://doi.org/10.1002/anie.201605909
14. Yang, D.; Li, P.; Zou, Y.; Cao, M.; Hu, H.; Zhong, Q.; Hu, J.; Sun, B.; Duhm, S.; Xu, Y.; et al. Interfacial Synthesis of Monodisperse $CsPbBr_3$ Nanorods with Tunable Aspect Ratio and Clean Surface for Efficient Light-Emitting Diode Applications. *Chem. Mater.* **2019**, *31*, 1575-1583, doi:10.1021/acs.chemmater.8b04651.
15. Cui, J.; Liu, Y.; Deng, Y.; Lin, C.; Fang, Z.; Xiang, C.; Bai, P.; Du, K.; Zuo, X.; Wen, K.; et al. Efficient light-emitting diodes based on oriented perovskite nanoplatelets. *Science Adv.* **2021**, *7*, eabg8458, doi:doi:10.1126/sciadv.abg8458.
16. Jurow, M.J.; Morgenstern, T.; Eisler, C.; Kang, J.; Penzo, E.; Do, M.; Engelmayer, M.; Osowiecki, W.T.; Bekenstein, Y.; Tassone, C.; et al. Manipulating the Transition Dipole Moment of $CsPbBr_3$ Perovskite Nanocrystals for Superior Optical Properties. *Nano Lett.* **2019**, *19*, 2489-2496, doi:10.1021/acs.nanolett.9b00122.
17. Walters, G.; Haeberlé, L.; Quintero-Bermudez, R.; Brodeur, J.; Kéna-Cohen, S.; Sargent, E.H. Directional Light Emission from Layered Metal Halide Perovskite Crystals. *J. Phys. Chem. Lett.* **2020**, *11*, 3458-3465, doi:10.1021/acs.jpclett.0c00901.
18. Hoang, M.T.; Pannu, A.S.; Yang, Y.; Madani, S.; Shaw, P.; Sonar, P.; Tesfamichael, T.; Wang, H. Surface Treatment of Inorganic $CsPbI_3$ Nanocrystals with Guanidinium Iodide for Efficient Perovskite Light-Emitting Diodes with High Brightness. *Nano-Micro Lett.* **2022**, *14*, 69, doi:10.1007/s40820-022-00813-9.
19. Kim, Y.-H.; Zhai, Y.; Lu, H.; Pan, X.; Xiao, C.; Gaulding, E.A.; Harvey, S.P.; Berry, J.J.; Vardeny, Z.V.; Luther, J.M.; et al. Chiral-induced spin selectivity enables a room-temperature spin light-emitting diode. *Science* **2021**, *371*, 1129-1133, doi:doi:10.1126/science.abf5291.
20. Li, H.; Lin, H.; Ouyang, D.; Yao, C.; Li, C.; Sun, J.; Song, Y.; Wang, Y.; Yan, Y.; Wang, Y.; et al. Efficient and Stable Red Perovskite Light-Emitting Diodes with Operational Stability >300 h. *Adv. Mater.* **2021**, *33*, 2008820, doi:https://doi.org/10.1002/adma.202008820.
21. Tang, Y.; Cao, X.; Honarfar, A.; Abdellah, M.; Chen, C.; Avila, J.; Asensio, M.-C.; Hammarström, L.; Sa, J.; Canton, S.E.; et al. Inorganic Ions Assisted the Anisotropic Growth of $CsPbCl_3$ Nanowires with Surface Passivation Effect. *ACS Appl. Mater. Interf.* **2018**, *10*, 29574-29582, doi:10.1021/acsami.8b09113.
22. Protesescu, L.; Yakunin, S.; Bodnarchuk, M.I.; Krieg, F.; Caputo, R.; Hendon, C.H.; Yang, R.X.; Walsh, A.; Kovalenko, M.V. Nanocrystals of Cesium Lead Halide Perovskites ($CsPbX_3$, X = Cl, Br, and I): Novel Optoelectronic Materials Showing Bright Emission with Wide Color Gamut. *Nano Lett.* **2015**, *15*, 3692-3696, doi:10.1021/nl5048779.
23. Lu, M.; Guo, J.; Sun, S.; Lu, P.; Wu, J.; Wang, Y.; Kershaw, S.V.; Yu, W.W.; Rogach, A.L.; Zhang, Y. Bright $CsPbI_3$ Perovskite Quantum Dot Light-Emitting Diodes with Top-Emitting Structure and a Low Efficiency Roll-Off Realized by Applying Zirconium Acetylacetonate Surface Modification. *Nano Lett.* **2020**, *20*, 2829-2836, doi:10.1021/acs.nanolett.0c00545.
24. Zhu, Y.; Zhao, J.; Yang, G.; Xu, X.; Pan, G. Ammonium acetate passivated $CsPbI_3$ perovskite nanocrystals for efficient red light-emitting diodes. *Nanoscale* **2020**, *12*, 7712-7719, doi:10.1039/D0NR01378A.
25. Pan, G.; Bai, X.; Yang, D.; Chen, X.; Jing, P.; Qu, S.; Zhang, L.; Zhou, D.; Zhu, J.; Xu, W.; et al. Doping Lanthanide into Perovskite Nanocrystals: Highly Improved and Expanded Optical Properties. *Nano Lett.* **2017**, *17*, 8005-8011, doi:10.1021/acs.nanolett.7b04575.

26. Yao, J.-S.; Ge, J.; Wang, K.-H.; Zhang, G.; Zhu, B.-S.; Chen, C.; Zhang, Q.; Luo, Y.; Yu, S.-H.; Yao, H.-B. Few-Nanometer-Sized α-$CsPbI_3$ Quantum Dots Enabled by Strontium Substitution and Iodide Passivation for Efficient Red-Light Emitting Diodes. *J. Am. Chem. Soc.* **2019**, *141*, 2069-2079, doi:10.1021/jacs.8b11447.
27. Xia, W.; Ren, Z.; Zheng, Z.; Luo, C.; Li, J.; Ma, W.; Zhou, X.; Chen, Y. Highly stable lanthanide-doped $CsPbI_3$ perovskite nanocrystals with near-unity quantum yield for efficient red light-emitting diodes. *Nanoscale* **2023**, *15*, 1109-1118, doi:10.1039/D2NR06317D.
28. Shen, X.; Zhang, Y.; Kershaw, S.V.; Li, T.; Wang, C.; Zhang, X.; Wang, W.; Li, D.; Wang, Y.; Lu, M.; et al. Zn-Alloyed $CsPbI_3$ Nanocrystals for Highly Efficient Perovskite Light-Emitting Devices. *Nano Lett.* **2019**, *19*, 1552-1559, doi:10.1021/acs.nanolett.8b04339.
29. Chen, D.; Ko, P.K.; Li, C.H.A.; Zou, B.; Geng, P.; Guo, L.; Halpert, J.E. Amino Acid-Passivated Pure Red $CsPbI_3$ Quantum Dot LEDs. *ACS Energy Lett.* **2023**, *8*, 410-416, doi:10.1021/acsenergylett.2c02243.
30. Jurow, M.J.; Lampe, T.; Penzo, E.; Kang, J.; Koc, M.A.; Zechel, T.; Nett, Z.; Brady, M.; Wang, L.-W.; Alivisatos, A.P.; et al. Tunable Anisotropic Photon Emission from Self-Organized $CsPbBr_3$ Perovskite Nanocrystals. *Nano Lett.* **2017**, *17*, 4534-4540, doi:10.1021/acs.nanolett.7b02147.
31. Barnes, W.L. Fluorescence near interfaces: The role of photonic mode density. *J. Modern Optics* **1998**, *45*, 661-699, doi:10.1080/09500349808230614.
32. Jeon, S.; Zhao, L.; Jung, Y.-J.; Kim, J. W.; Kim, S.-Y.; Kang, H.; Jeong, J.-H.; Rand, B. P.; Lee, J.-H. Perovskite Light-Emitting Diodes with Improved Outcoupling Using a High-Index Contrast Nanoarray, *Small* **2019**, 15, 1900135, doi.org/10.1002/smll.201900135
33. He, S.; Kumar, N.; Lee, H. B.; Ko, K.-J.; Jung, Y.-J.; Kim, J. I.; Bae, S.; Lee, J.-H.; Kang, J.-W. Tailoring the refractive index and surface defects of CsPbBr3 quantum dots via alkyl cation-engineering for efficient perovskite light-emitting diodes, *Chem. Eng. J.* **2021**, 425, 130678, doi.org/10.1016/j.cej.2021.130678
34. Cheon, H. J.; Woo, S.-J.; Baek, S.-H.; Lee, J.-H.; Kim, Y.-H. Dense Local Triplet States and Steric Shielding of Multi-Resonance TADF Emitter Enable High-Performance Deep Blue OLEDs, *Adv. Mater.* **2022**, 34, 2207416, doi.org/10.1002/adma.202207416.